Progress In Electromagnetics Research, PIER 24, 279–310, 1999

FULL-WAVE ANALYSIS OF A FABRY-PEROT TYPE RESONATOR

D. I. Kaklamani

Department of Electrical and Computer Engineering
National Technical University of Athens
9 Iroon Polytechniou Str.
15780 Zografos, Athens, Greece

1. INTRODUCTION

The analysis of open resonators consisting of two parallel orthogonal parallelepiped conductors has been among the first to be carried out by computer techniques, approximately 40 years ago [1]. The semi-open nature of the parallel plate resonator eliminates large number of possible modes, which would be rapidly damped by the radiation from the open sides [2], keeping only longitudinal resonances. This fact has played an essential role in the development of laser systems at optical frequencies and the construction of active quantum electronic devices. The system of parallel plate reflectors has been used for very long in the classical Fabry-Perot interferometer [3] and this is why it is usually referred to as Fabry-Perot resonator. Indeed, Fabry-Perot interferometers of a metal-dielectric-metal configuration have been widely used as bandpass optical filters and laser resonators [4–6]. Recently, there has been a continuously increasing interest of using Fabry-Perot structures

as a wavemeter at microwave and millimetre wavelength frequencies [7–10], as well as to determine the material properties of high temperature superconductors [11–16]. Similar open type structures are proposed to be used at sub-millimetre wavelengths where, contrary to the optical wavelengths, the resonator dimensions are comparable to the operation wavelengths. In this case, it is required to compute the resonance properties of low order modes in the Fabry-Perot type structures. The same statements are valid for optical microresonators where, again, low order modes are employed.

In this paper, an open resonator of the type shown in Figure 1(a), consisting of two equal parallel plates and excited by an elementary dipole parallel to the plates, is examined. This structure is directly related to the famous Casimir effect [17, 18], which exhibits the vacuum energy of the electromagnetic field as a weak attraction force between two uncharged perfectly conducting plates very close to each other. The existence of this force, which is linked with fundamental concepts of physics, such as virtual particles and zero energy fluctuations, has recently re-attracted much interest and was confirmed by a very accurately designed experiment by Lamoreaux [19].

The analysed structure shown in Figure 1(a) is derived as a special case of the Q-number of perfectly conducting parallel rectangular plates—or equivalently the case of Q-number of rectangular apertures "cut" on parallel infinite screens—shown in Figure 1(b). Actually, this multi-plate problem has been addressed in a series of papers [20–22], by extending the work presented in [23] for a single rectangular conducting plate and using High Performance Computing (HPC) merely as a computational tool to reduce drastically the consumed CPU time. Therefore, according to the pursued analysis, the two plates shown in Figure 1(a) could be displaced and/or not necessarily of the same dimensions. Furthermore, the pursued analysis can be easily extended to the case of multi Fabry-Perot resonators, taking into account coupling phenomena between closely spaced resonators.

In section 2, the formulation of the multi-plate problem is presented and a system of coupled integral equations is derived in terms of the conductivity currents induced on the parallel displaced rectangular conducting plates surfaces. The system of integral equations is solved in section 3, using a Method of Moments (MoM) and in particular a Galerkin technique. Entire domain Chebyshev type basis functions incorporating the current edge behaviour [24], which have been proved

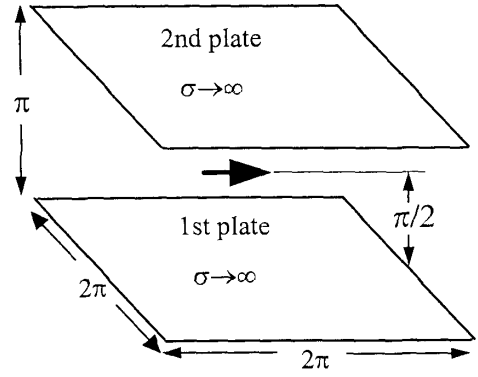

Figure 1(a). Two parallel plates open resonator excited by a Hertzain dipole: $x_0 = y_0 = 0$.

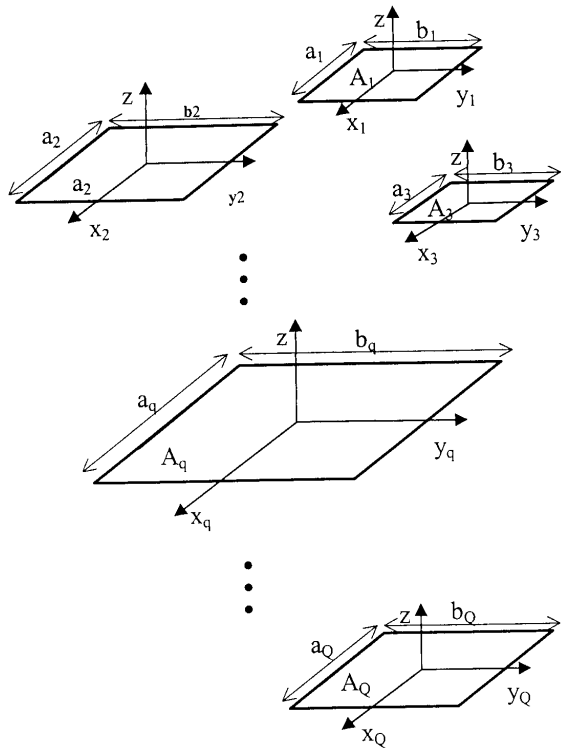

Figure 1(b). Q-number of perfectly conducting parallel rectangular plates.

very efficient in previous works [23, 25], are employed to describe the unknown currents on the plates. Numerical results are presented in section 4 for several resonator sizes and operation frequencies, while concluding remarks and topics for further work are given in section 5.

In the following, an $\exp(j\omega t)$ time dependence is assumed and suppressed throughout the analysis. The main emphasis is given to near-field quantities, such as the conductivity currents distribution on the plates surface.

2. FORMULATION OF THE INTEGRAL EQUATIONS

The analysis presented in [23] is extended for the case of Q-number of perfectly conducting infinitesimal thickness plates, placed at arbitrary positions and orientations on parallel planes—or equivalently the case of Q-number of rectangular apertures "cut" on parallel infinite screens—as shown in Figure 1(b), which are illuminated by an external source with known pattern. For the purpose of the present analysis, the multi-plate structure is illuminated by a primary field

$$\underline{E}_0(\underline{r}, \underline{r}_0) = m_\ell \delta \cdot \overline{\overline{G}}(\underline{r}, \underline{r}_0) \tag{1}$$

which is created by a parallel to the xy-plane Hertzian dipole, with orientation vector

$$\hat{\delta} = \cos\varphi_\delta \hat{\mathrm{x}} + \sin\varphi_\delta \hat{\mathrm{y}} \qquad 0 \le \varphi_\delta \le 2\pi \tag{2}$$

position vector

$$\underline{r}_0 = (x_0, y_0, \delta) \qquad -\infty < x_0, y_0 < +\infty \tag{3}$$

and electric moment $m_\ell = I\ell\,, \ell$ being the dipole length and I being the constant current flowing on the dipole surface. Alternatively, for a plane wave incidence, the primary field is given by

$$\underline{E}_0(\underline{r}) = E_0 \hat{e} \exp(-jk_0 \hat{k}_i \cdot \underline{r}) \tag{4}$$

where $\hat{e} = (\cos\varphi_e \hat{x} + \sin\varphi_e \hat{y})\sin\theta_e + \cos\theta_e \hat{z}$ and $\hat{k}_i = k_{ix}^{\mu}\hat{x} + k_{iy}^{\mu}\hat{y} + k_{iz}^{\mu}\hat{z}$ are the unit vectors denoting the polarisation and incidence directions respectively and E_0 is the assumed unit plane wave amplitude.

Applying the Green's theorem, the electric field is expressed as a summation of the primary excitation $\underline{E}_0(\underline{r})$ (Hertzian dipole or plane

wave given by eqs (1) or (4) respectively) and its distortions due to the presence of the conducting plates, as

$$\begin{aligned}\underline{E}(\underline{r},\underline{r}_0) = \underline{E}_0(\underline{r},\underline{r}_0) &- j\omega\mu_0 \iint\limits_{A_1} d\underline{r}'_1 \overline{G}(\underline{r},\underline{r}'_1)\cdot\underline{J}_1(\underline{r}'_1)\\ &- j\omega\mu_0 \iint\limits_{A_2} d\underline{r}'_2 \overline{G}(\underline{r},\underline{r}'_2)\cdot\underline{J}_2(\underline{r}'_2)\\ &- \ldots - j\omega\mu_0 \iint\limits_{A_q} d\underline{r}'_q \overline{G}(\underline{r},\underline{r}'_q)\cdot\underline{J}_q(\underline{r}'_q)\\ &- \ldots - j\omega\mu_0 \iint\limits_{A_Q} d\underline{r}'_Q \overline{G}(\underline{r},\underline{r}'_Q)\cdot\underline{J}_Q(\underline{r}'_Q) \qquad (5)\end{aligned}$$

where the negative sign of the right hand side terms is due to the $\exp(+j\omega t)$ time dependence, $A_q = a_q \times b_q$, ($q = 1, 2, \ldots, Q$) is the finite zero-thickness q-th conducting plate surface, $\underline{r}'_q = (x'_q, y'_q, z'_q = 0)$ denotes the position vector of an arbitrary point on A_q with respect to the local cartesian coordinates system attached to the q-th plate centre of gravity, $\underline{J}_q(\underline{r}'_q)$ denotes the unknown current density on the q-th plate and

$$\overline{G}(\underline{r},\underline{r}'_q) = (\overline{I} + k_0^{-2}\nabla\nabla)\frac{\exp(-jk_0|\underline{r}-\underline{r}'_q|)}{4\pi|\underline{r}-\underline{r}'_q|} \qquad (6)$$

is the free-space dyadic Green's function, which satisfies the wave equation

$$\nabla\times\nabla\times\overline{G}(\underline{r},\underline{r}'_q) - k_0^2(\underline{r})\overline{G}(\underline{r},\underline{r}'_q) = \overline{I}\delta(\underline{r}-\underline{r}'_q) \qquad (7)$$

$k_0 = \omega\sqrt{\varepsilon_0\mu_0}$ being the free space propagation constant, ω being the angular frequency, $\overline{I} = \hat{x}\hat{x} + \hat{y}\hat{y} + \hat{z}\hat{z}$ being the unit dyadic and $\delta(\underline{r})$ being the three-dimensional delta function.

If the observation point is placed on each conductor surface $A_q = a_q \times b_q$ and the short circuit boundary conditions $\hat{z}\times\underline{E}(\underline{r}_q) = 0$ are satisfied, a system of Q-two-dimensional integral equations is derived in terms of the currents $\underline{J}_q = J_{q_x}\hat{x} + J_{q_y}\hat{y}$, as

$$\sum_{q=1}^{Q}\iint\limits_{A_q} d\underline{r}'_q \overline{K}_{pq}(\underline{r},\underline{r}'_q)\cdot\underline{J}_q(\underline{r}'_q) = \underline{R}_p(\underline{r}) \qquad (p = 1, 2, \ldots, Q) \qquad (8)$$

where the subscript q $(q = 1, 2, \ldots, Q)$, wherever used, denotes the q-th plate, $\overline{\underline{K}}_{pq}$ are known kernel matrix functions incorporating the free-space dyadic Green's function and the known right hand vectors $\underline{R}_p$ describe the primary excitation impact. The form of the $\overline{\underline{K}}_{pq}$ kernel functions depend exclusively on the geometry of the structure (i.e., the dimensions and the relative position of the plates), while the $\underline{R}_p$ right hand functions depend on the type of the external source.

3. SOLUTION VIA ENTIRE DOMAIN GALERKIN TECHNIQUE

The system of integral equations (8) is solved by employing an entire domain Galerkin technique [26], where the unknown vector quantities $\underline{J}_q(\underline{r}'_q)$ should be expanded in terms of linearly independent "appropriate" basis functions [24–29]. To this end, Chebyshev type series with convenient arguments, incorporating the current edge behaviour, which have been proved very efficient in previous works [23, 25], are employed. Therefore, with respect to the local cartesian coordinates system (x_q, y_q), attached to the q-th plate centre of gravity $(q = 1, 2, \ldots, Q)$, the corresponding transverse conductivity currents are expressed as

$$\begin{aligned} J_{q_x}(\underline{r}_q) &= s(x_q, y_q) \sum_{n=0}^{N_q} \sum_{m=0}^{M_q} c_{q_{nm}} \Phi_{q_{nm}}(x_q, y_q) \\ &= s(x_q, y_q) \sum_{n=0}^{N_q} \sum_{m=0}^{M_q} c_{q_{nm}} U_n\left(\frac{2x_q}{a_q}\right) T_m\left(\frac{2y_q}{b_q}\right) \qquad (9.1) \\ J_{q_x}(\underline{r}_q) &= \frac{1}{s(x_q, y_q)} \sum_{n=0}^{N_q} \sum_{m=0}^{M_q} d_{q_{nm}} \Xi_{q_{nm}}(x_q, y_q) \\ &= \frac{1}{s(x_q, y_q)} \sum_{n=0}^{N_q} \sum_{m=0}^{M_q} d_{q_{nm}} U_m\left(\frac{2y_q}{b_q}\right) T_n\left(\frac{2x_q}{a_q}\right) \qquad (9.2) \end{aligned}$$

where T_n and U_n are the n-th order Chebyshev polynomials of the first and second kind respectively, whose arguments are chosen in a way that the appropriate stationary waves are developed on the conducting plates surfaces,

$$s(x_q, y_q) = \sqrt{\frac{1 - (2x_q/a_q)^2}{1 - (2y_q/b_q)^2}} \qquad (q = 1, 2, \ldots, Q) \qquad (10)$$

is a square root term, which satisfies [30–32] the edge conditions [24] at $x_q = \pm a_q/2\,,\ y_q = \pm b_q/2\,,$ accelerating significantly the convergence of the proposed Galerkin technique [25] and $c_{q_{nm}}$ and $d_{q_{nm}}$ are the unknown coefficients to be determined.

Taking into consideration the $\exp(+j\omega t)$ time dependence, the Fourier expansion of the scalar Green's function

$$\frac{\exp(-jk_0|\underline{r}-\underline{r}'_q|)}{4\pi|\underline{r}-\underline{r}'_q|} = \frac{1}{(2\pi)^3}\lim_{\varepsilon\to 0^+}\int_{-\infty}^{+\infty}dk_x\int_{-\infty}^{+\infty}dk_y\int_{-\infty}^{+\infty}dk_z\frac{\exp(j\underline{k}\cdot(\underline{r}-\underline{r}'_q))}{k^2-k_0^2+j\varepsilon} \tag{11}$$

where $\underline{k} = (k_x, k_y, k_z)$ and $k^2 = k_x^2 + k_y^2 + k_z^2$ is employed and the MoM is further applied by multiplying each one of eqs (8) by the vector quantity

$$s(x_q,y_q)\Phi_{n'm'}(x_q,y_q)\hat{x} + \frac{1}{s(x_q,y_q)}\Xi_{n'm'}(x_q,y_q)\hat{y} \qquad (n'=0,1,\ldots,N_q;\ m'=0,1,\ldots,M_q) \tag{12}$$

and integrating on the q-th conducting plate surface A_q $(q = 1, 2\ldots, Q)$. All the integrals over A_q are computed analytically making use of the formula [33]

$$\int_{-a/2}^{+a/2}dt\frac{\exp(jwt)}{\sqrt{1-(2t/a)^2}}T_v(2t/a) = \frac{a}{2}\pi j^v J_v(wa/2) \tag{13.1}$$

$$\int_{-a/2}^{+a/2}dt\exp(jwt)\sqrt{1-(2t/a)^2}U_v(2t/a) = \frac{a}{2}\pi j^v(v+1)\frac{J_{v+1}(wa/2)}{wa/2} \tag{13.2}$$

$J_v(x)$ being the v-th order cylindrical Bessel function of the first kind, while, in order to enable the analytical computation of the k_z-integrals, the tangential electric field is assumed to vanish "slightly above" the q-th conducting plate surface A_q, by setting $r_q = (x_q, y_q, \delta_q)$ with

$\delta_q \rightarrow 0^+ \quad (q = 1, 2, \ldots, Q)$. Because of this approximation, all the derived integrals with respect to the k_z variable are of the type

$$\lim_{\varepsilon \rightarrow 0^+} \int_{-\infty}^{+\infty} dk_z \frac{f(k_z)}{k^2 - k_0^2 + j\varepsilon} \exp(j\alpha k_z) \qquad \alpha \neq 0 \tag{14}$$

having poles at the points $\pm q_0$ with $q_0^2 = k_0^2 - k_x^2 - k_y^2 - j\varepsilon\,,\ \varepsilon \rightarrow 0^+$ and, therefore, their values are computed by employing the Cauchy theorem. In each case, the contour is closed depending on the number α sign. Then, all the double integrals with respect to the variables k_x and k_y are numerically computed, after being transformed in cylindrical coordinates, as

$$\int_{-\infty}^{+\infty} dk_x \int_{-\infty}^{+\infty} dk_y \equiv \int_0^{+\infty} d\rho_k \rho_k \int_0^{2\pi} d\varphi_k \equiv \iint_{\Omega_k} d\underline{\tilde{k}}$$

$$\underline{\tilde{k}} = k_x \hat{x} + k_y \hat{y} = \rho_k (\cos\varphi_k \hat{x} + \sin\varphi_k \hat{y}) \tag{15}$$

In this way, the convergence of the involved integrals has to be examined only for $\rho_k \rightarrow +\infty$. As it is shown in [25], the above described approximation concerning the $\delta_q \rightarrow 0^+$ factor enables also the convergence of the ρ_k-integrals without having noticeable impact on the final results. Note that, since exponential terms $\exp(-jtq_0)$ with $t \geq 0$ are included in each of the integrands, in accordance to the $\exp(j\omega t)$ time dependence and the satisfaction of the radiation condition at infinity, it is required that

$$\text{Real}\,(q_0) > 0 \quad \text{and} \quad \text{Imag}\,(q_0) < 0 \quad \text{with} \quad q_0 = \sqrt{k_0^2 - \rho_k^2} \tag{16}$$

Finally, after applying the Galerkin technique, a $\sum_{q=1}^{Q} 2(N_q+1)\ (M_q+1)$ order linear system of equations is derived, in terms of $c_{q_{nm}}$ and $d_{q_{nm}}\ \ (q = 1, 2, ..., Q)$, as

$$\sum_{q=1}^{Q} \overline{\underline{X\Psi}}_{pq} \cdot \underline{cd}_q = \underline{X\Psi}_p^0 \qquad (p = 1, 2, \ldots, Q) \tag{17}$$

where all the involved submatrices are defined in the Mathematical Appendix, the elements of the unknown vectors $\underline{cd}_q = [\,\underline{c}_q \,|\, \underline{d}_q\,]^T$ are

the unknown coefficients $c_{q_{nm}}$ and $d_{q_{nm}}$ to be determined and the position of each submatrice element is defined by transforming the double pointers to simple ones. Note that, in all the expressions given in the Mathematical Appendix, special care has been taken in making the proper transformations from each local cartesian coordinates system attached to the q-th plate centre of gravity —denoted by the subscript q, as (x_q, y_q, z_q)—to a global cartesian coordinates system—denoted without any subscript, as (x, y, z), taking into account that the position vector of the q-th plate centre of gravity is denoted by the formula

$$\underline{r}_q^0 = x_q^0 \hat{x} + y_q^0 \hat{y} + z_q^0 \hat{z} \qquad (q = 1, 2, \ldots, Q) \tag{18}$$

with respect to a global system of coordinates (x, y, z).

The successful choice of the entire domain basis functions leads to quick convergence and small order systems (i.e., small N_q, M_q values). Therefore, the use of indirect methods is not needed and the system is numerically solved by employing the method of triangulation. Note that, all the system kernel elements are double integrals of the form $\int_0^{+\infty} d\rho_k \int_0^{2\pi} d\varphi_k$ given by eq. (15), which refer to the Green's function Fourier expansion and are numerically computed, by a 12-point quadrature Gauss algorithm [33], as in [23, 25]. Once the unknown coefficients are determined, the currents on the plates surfaces and the electric field in the near and far field region are computed, using the formula [33]

$$T_n(\cos\theta) = \cos(n\theta) \qquad U_n(\cos\theta) = \sin[(n+1)\theta]/\sin\theta \tag{19}$$

4. NUMERICAL RESULTS

Numerical calculations are carried out applying the analysis presented in the previous two sections. In order to calculate the conductivity currents induced on the plates surfaces and given by eqs (9) and (19), the unknown expansion coefficients $c_{q_{nm}}$ and $d_{q_{nm}}$ are determined by numerically solving the $\sum_{q=1}^{Q} 2(N_q+1)(M_q+1)$ order linear system of equations (17) via the method of triangulation. In calculating the kernel elements and the right hand side elements, all the involved double integrals $\iint_{\Omega_k} d\underline{\tilde{k}} \equiv \int_0^{+\infty} d\rho_k \rho_k \int_0^{2\pi} d\varphi_k$ appearing in eqs (A.1) and (A.4) of the Mathematical Appendix are numerically computed employing a 12-point quadrature Gauss integration algorithm [33]. The

only singularity point of the integrands is the $\rho_k = k_0$ branch point and the proper selection of the branch cut is determined by the satisfaction of the radiation conditions at the ρ_k-complex plane. Then, the convergence of the integrals value is checked with respect to both the ρ_k and φ_k subdivisions and the truncation of the ρ_k-integration upper limit. The right hand side integrands (A.4) exhibit an exponential behavior $e^{-\rho_k \mathrm{sgn}(\delta - z_p^0)(\delta - z_p^0 - \delta_p)}$ $(p = 1, 2, \ldots, Q)$ for $\rho_k \to \infty$ and, therefore, converge very fast, depending on the δ and z_p^0 relative values. Then, the approximation that is described in section 3 concerning the $\delta_q \to 0^+$ $(q = 1, 2, \ldots, Q)$ factor enables the convergence of the ρ_k-integrals (A.1) with respect to their upper limit in the regions $\varphi_k = \pm\varepsilon$, $\pi/2 \pm \varepsilon$, $\pi \pm \varepsilon$ and $3\pi/2 \pm \varepsilon$ with $0 < \varepsilon << 1$, whose surface becomes noticeable for large values of the ρ_k-variable. In these regions, the worst convergence is exhibited, as $e^{-\rho_k \delta_q}$. In all the results that are presented in this section, it is assumed that $k_0 \delta_q = 0.02$. Due to this assumption, although the final results (i.e., current distributions) are not affected more than 0.5%, the involved ρ_k-integrals can be truncated at $\rho_k = 500 k_0$, while an upper limit $\rho_k = 900 k_0$ is required for $k_0 \delta_q = 0.01$. The necessity of a relatively small value for the ρ_k-integration upper limit is also imposed, when considering that a further computational cost increase is caused, due to the fact that, all the (A.1) and (A.4) integrands vary more rapidly with the ρ_k increase. Therefore, when integrating with respect to the φ_k-variable, more subdivisions must be considered for large ρ_k values. It should also be noted that, since it has been numerically proved that the contribution to the ρ_k-integrals final value is much more significant at the beginning of the ρ_k-integration path, more dense ρ_k-subdivisions are needed for $0 \leq \rho_k \leq 20 k_0$, while these become much more sparse with the ρ_k increase.

After having ensured the convergence of the kernel elements and the right hand side elements of the linear system of equations (17), the convergence of the proposed method with respect to the system order $\sum_{q=1}^{Q} 2(N_q + 1)(M_q + 1)$, namely with respect to the truncation of the (9.1) and (9.2) expansion series (i.e., the M_q and N_q integers) is controlled by computing the conductivity current distributions. Probably, this convergence is expected to be accomplished more rapidly, when electrically small plates and/or electrically large distances between the plates and the emitting Hertzian dipole —or moreover a plane wave incidence— are considered. The convergence rate of near field quanti-

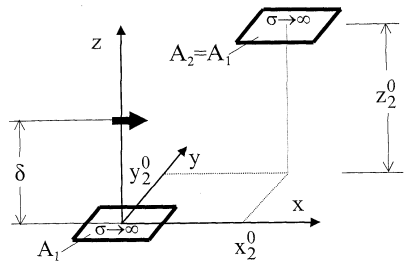

Figure 2. Two uncoupled electrically small identical plates illuminated by a Hertzian diploe parallel to the x-axis above the centre of the 1st plate: (a) geometry: $\underline{r}_1^0 = 0$, $k_0 a_1 = k_0 a_2 = 1$, $k_0 b_1 = k_0 b_2 = 0.25$, $\varphi_\delta = 0$, $k_0 x_0 = k_0 y_0 = 0$, $k_0 \delta = 2.1$ and different places of the 2nd plate along the $x = y = z$ line.

ties, such as the conductivity current distributions, is the most important result concerning the accuracy of the proposed method, because of the fact that both the radiation patterns being far field quantities and the input impedances being derived by an integration converge more rapidly. Therefore, for all the derived results that follow, extensive checks of the convergence in terms of the M_q and N_q integers are carried out and presented.

In order to have independent checks of the proposed method, numerical results are carried out for special cases and compared with previous works. To this end, a structure consisted of two conducting plates $(Q = 2)$ is considered (see Figure 2(a)). The global cartesian coordinates system coincides with the local cartesian coordinates system attached to the 1st plate centre of gravity, i.e., $\underline{r}_1^0 = 0$ and $(x, y, z) \equiv (x_1, y_1, z_1)$. The 2nd plate is placed very far from the 1st one, so that there is no coupling between the two plates and the derived results are compared with previously published data, concerning one conducting plate [23, 34, 35]. An indicative case concerning electrically small plates is shown in Figure 2, to be compared with Figure 3.5 of [34]. The plates are of equal dimensions $k_0 a_1 = k_0 a_2 = 1$ and $k_0 b_1 = k_0 b_2 = 0.25$, while a Hertzian dipole is radiating parallel to the x-axis $(\varphi_\delta = 0)$ above the centre of the 1st plate $(x_0 = y_0 = 0)$ at a vertical distance $k_0 \delta = 2.1$ (i.e., very close to the 1st plate). Starting from a distance $k_0 x_2^0 = k_0 y_2^0 = k_0 z_2^0 = 100$, the 2nd plate is moved

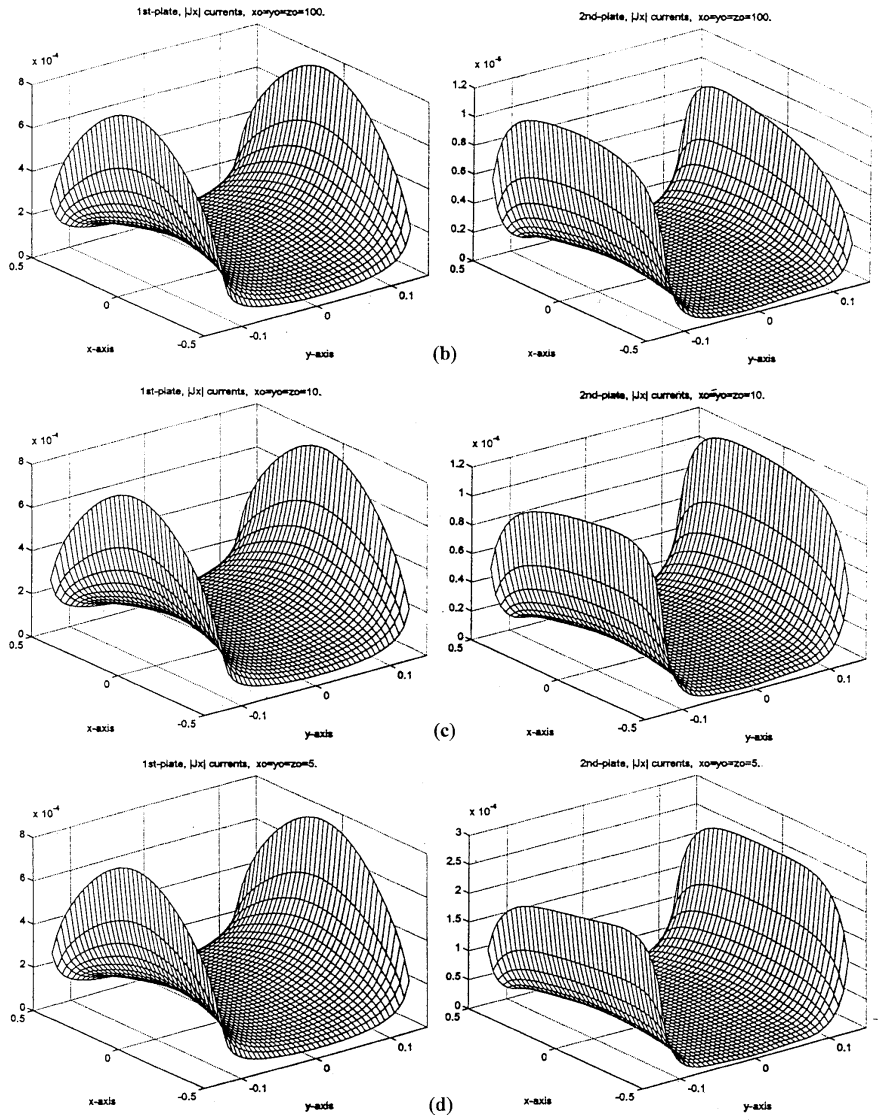

Figure 2. Two uncoupled electrically small identical plates illuminated by a Hertzian diploe parallel to the x-axis above the centre of the 1st plate: (b) co-polarised currents $|J_x|$ on both plates for $k_0x_2^0 = k_0y_2^0 = k_0z_2^0 = 100$ (c) co-polarised currents $|J_x|$ on both plates for $k_0x_2^0 = k_0y_2^0 = k_0z_2^0 = 10$ (d) co-polarised currents $|J_x|$ on both plates for $k_0x_2^0 = k_0y_2^0 = k_0z_2^0 = 5$.

towards the 1st one along the $x = y = z$ line (keeping always the primary source at the same position) and in Figure 2 the co-polarised currents $|J_x|$ induced on both plates are plotted for different places of the 2nd plate. Due to the electrically small dimensions of both plates, even for $k_0x_2^0 = k_0y_2^0 = k_0z_2^0 = 5$, no coupling between the two plates is exhibited and the conductivity currents are only affected by the plates distance from the Hertzian dipole; therefore, only the 2nd plate currents alter in Figure 2. In all cases, detailed convergence test are carried out, which are not presented here. The cross-polarised currents $|J_y|$ converge more slowly than the co-polarised ones $|J_x|$. Nevertheless, as expected, the cross-polarised currents are one order of magnitude smaller than the corresponding co-polarised ones on each plate, while the currents excited on the 2nd plate start from being also one order of magnitude smaller than the corresponding ones induced on the much closer to the primary source 1st plate and gradually increase as the 2nd plate approaches the 1st one (and the excitation). The validity of the code is further checked by considering a case symmetrical to the one presented in Figure 2(d). This is done by moving the 2nd plate at $k_0x_0 = k_0y_0 = 5$ and $k_0\delta = 5 - 2.1 = 2.9$ and getting for the 2nd plate the current distributions which corresponded to the 1st plate in Figure 2(d) and vise versa. Then, moving to structures like the one shown in Figure 1(a), the 2nd plate is placed concentrically to the 1st one at $k_0x_2^0 = k_0y_2^0 = 0$ and $k_0z_2^0 = 5$. Nevertheless, the electrically small dimensions of both plates prevent the structure from behaving like an open resonator, namely "trapping" part of the radiating energy in-between the two plates region. In order to achieve a resonating behavior, it is necessary to move to electrically larger dimensions, which is done in the following. However, dealing with electrically larger structures would lead to practically prohibitive computational cost, both in terms of memory requirement and CPU time, since more basis functions (i.e., larger M_q and M_q values) would be needed to achieve the same order of accuracy. This problem is encountered using parallel processing techniques, extensively discussed in [20–22].

As already mentioned in the introductory section, the specific case of two parallel concentric plates (i.e., $Q = 2$ and $(x_1, y_1) \equiv (x_2, y_2)$), consisting a Fabry-Perot type open resonator, is of special importance. In Figure 1(a), the specific examined geometry is shown. The open resonator system is excited by a Hertzian dipole placed in the middle of the distance between the two plates ($x_0 = y_0 = 0$, $\delta = \pi/2$),

whereas the plates dimensions are $a_q \times b_q = 2\pi \times 2\pi \quad (q = 1, 2)$. Due to the examined structure symmetry, the conductivity currents distribution induced on the two plates surfaces is identical. In order to compute the system kernel phase space double integrals, the 12-point quadrature Gauss algorithm is parallelised, by subdividing the integration path and splitting the corresponding calculations on to different processors of the parallel machine. The resulting parallel algorithm is computed exhibiting considerable speedups, for plates with dimensions of multiple wavelengths. Due to the inherent parallel nature of the proposed MoM, the results are obtained with minimal additional to the sequential code programming effort [20–23]. Then, the computation times become tolerable, allowing for the problem size, hence the accuracy, to be increased. The numerical results presented in Figures 3–5 are performed on a shared-memory Silicon Graphics Power Challenge with 14 TFP processors. The convergence of the conductivity current distributions is in any case better than 5%, whereas the convergence rate depends on the problem size, namely the product of the frequency times the most critical dimension (plates sizes or dipole-plates distance). This convergence in terms of $N_1 = N_2 = N = M_1 = M_2 = M$ is shown in Figures 3, 4 and 5 for three different operation frequencies $k_0 = 1$, 2 and 3 respectively. As expected, the dominant co-polarised J_x currents converge faster than the cross-polarised J_y ones, which are in any case one order of magnitude smaller. Furthermore, it is clear that, as already mentioned, more basis functions are needed for higher frequencies. In Figure 6, the resonance behaviour of the examined structure is exhibited by plotting the J_x currents, sweeping the frequency from $k_0 = 0.1$ to $k_0 = 2$ (with more detailed presentation around the resonance region $k_0 = 1$), while Figure 7 summarises the open resonator results for the same frequency region.

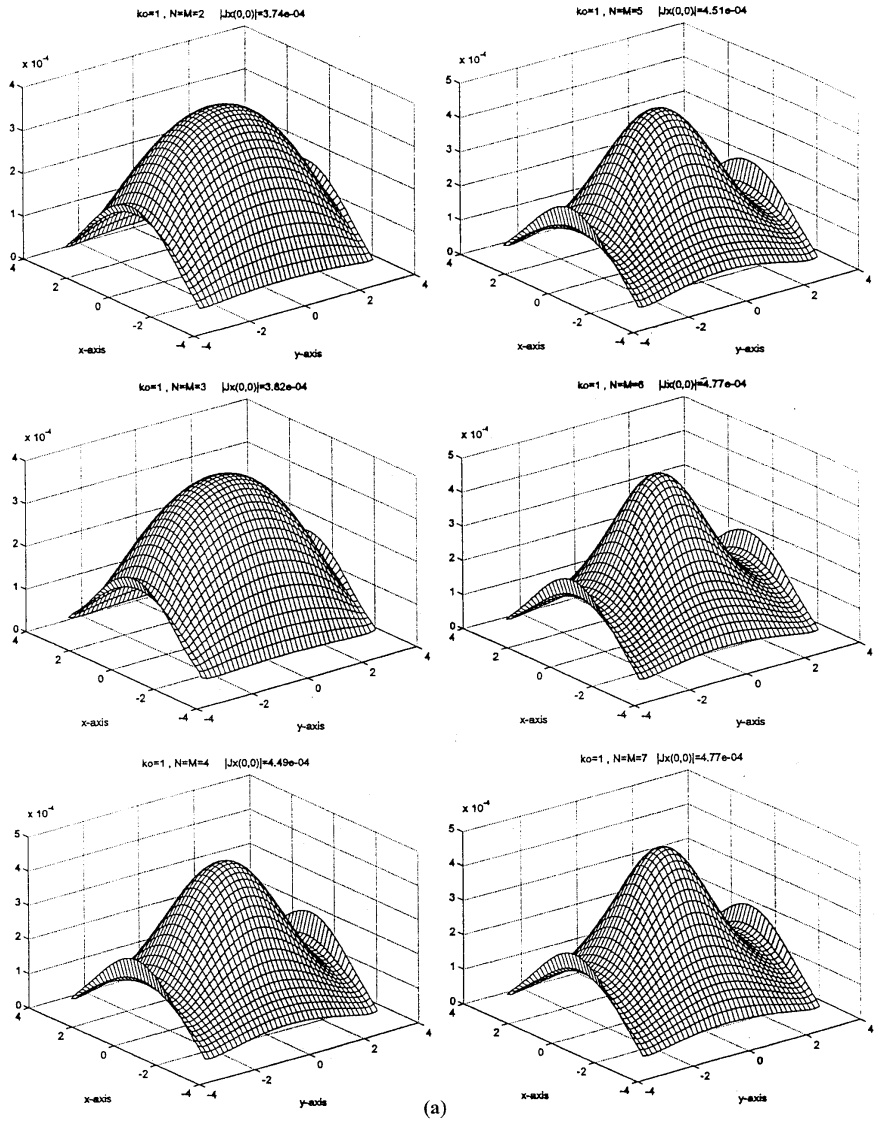

Figure 3. Convergence of the conductivity currents induced on each plate of the open resonator shown in Figure 1(a), for $k_0 = 1$: (a) co-polarised $|J_x|$ currents.

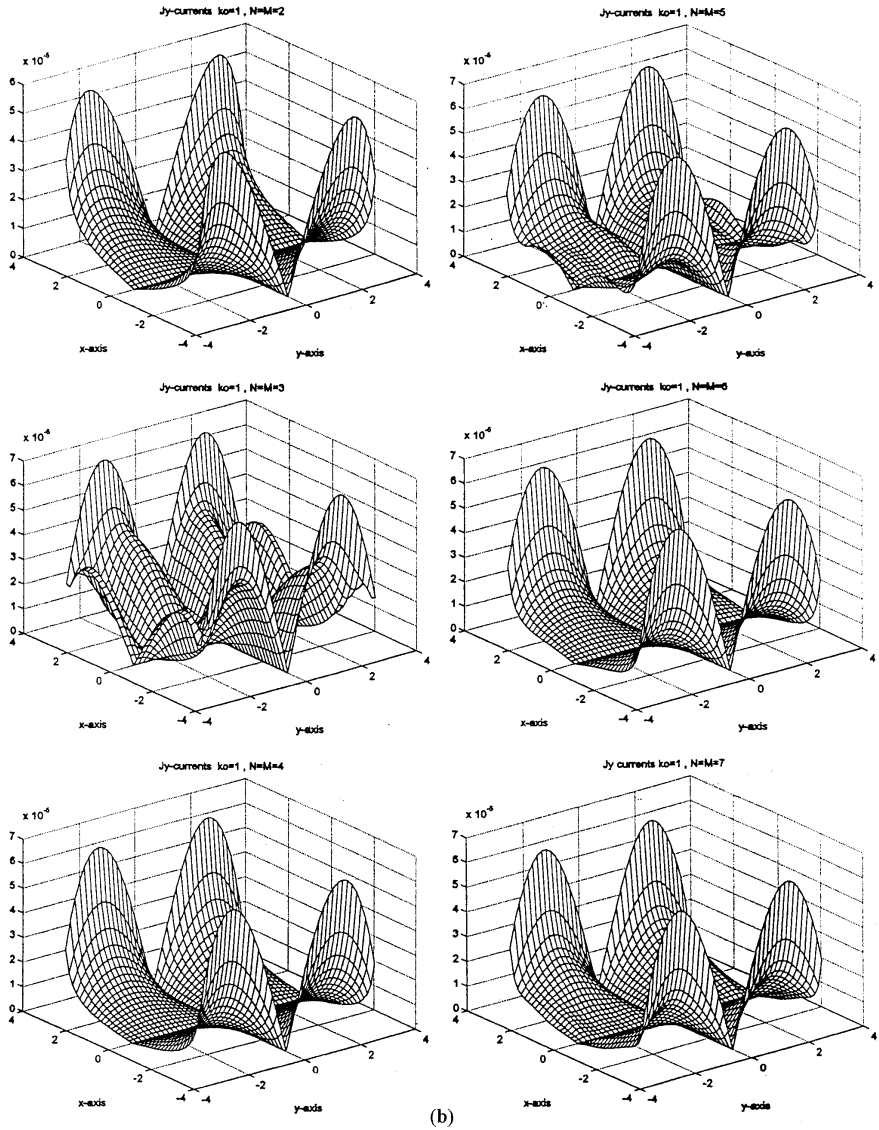

Figure 3. Convergence of the conductivity currents induced on each plate of the open resonator shown in Figure 1(a), for $k_0 = 1$: (b) cross-polarised $|J_y|$ currents.

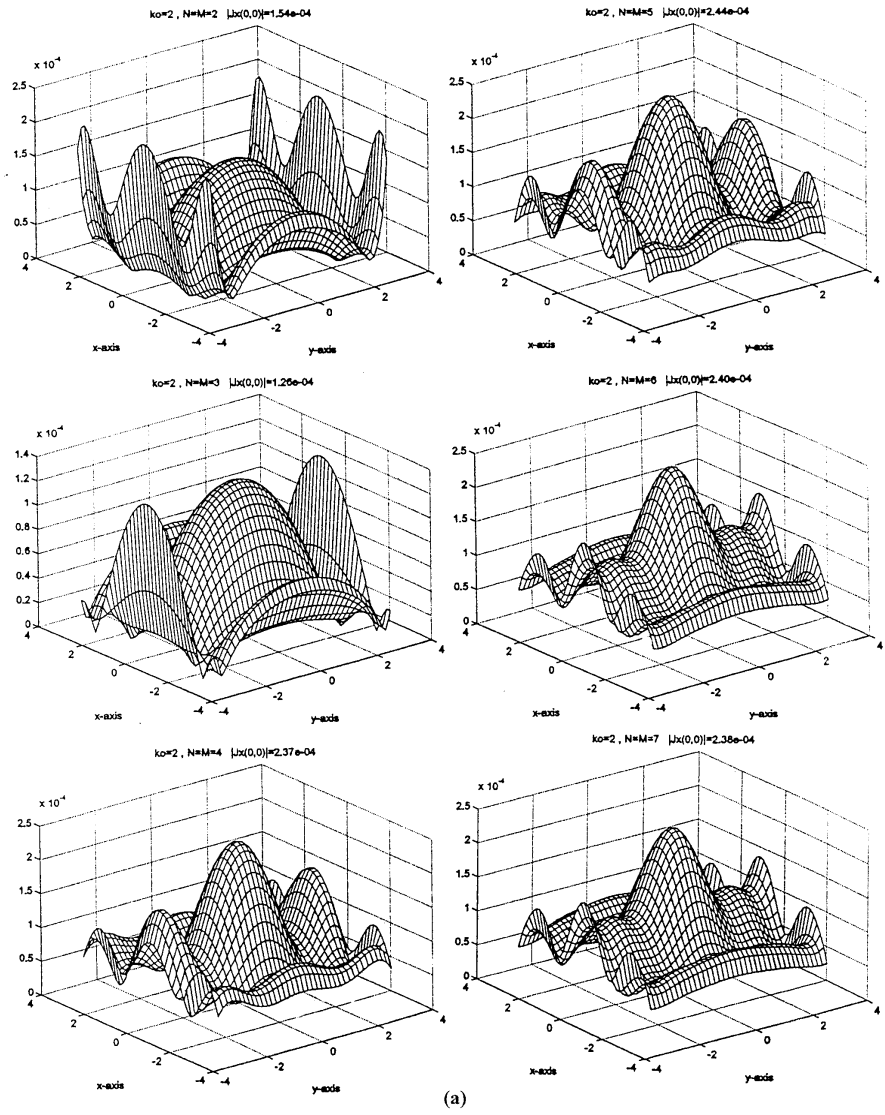

Figure 4. Convergence of the conductivity currents induced on each plate of the open resonator shown in Figure 1(a), for $k_0 = 2$: (a) co-polarised $|J_x|$ currents.

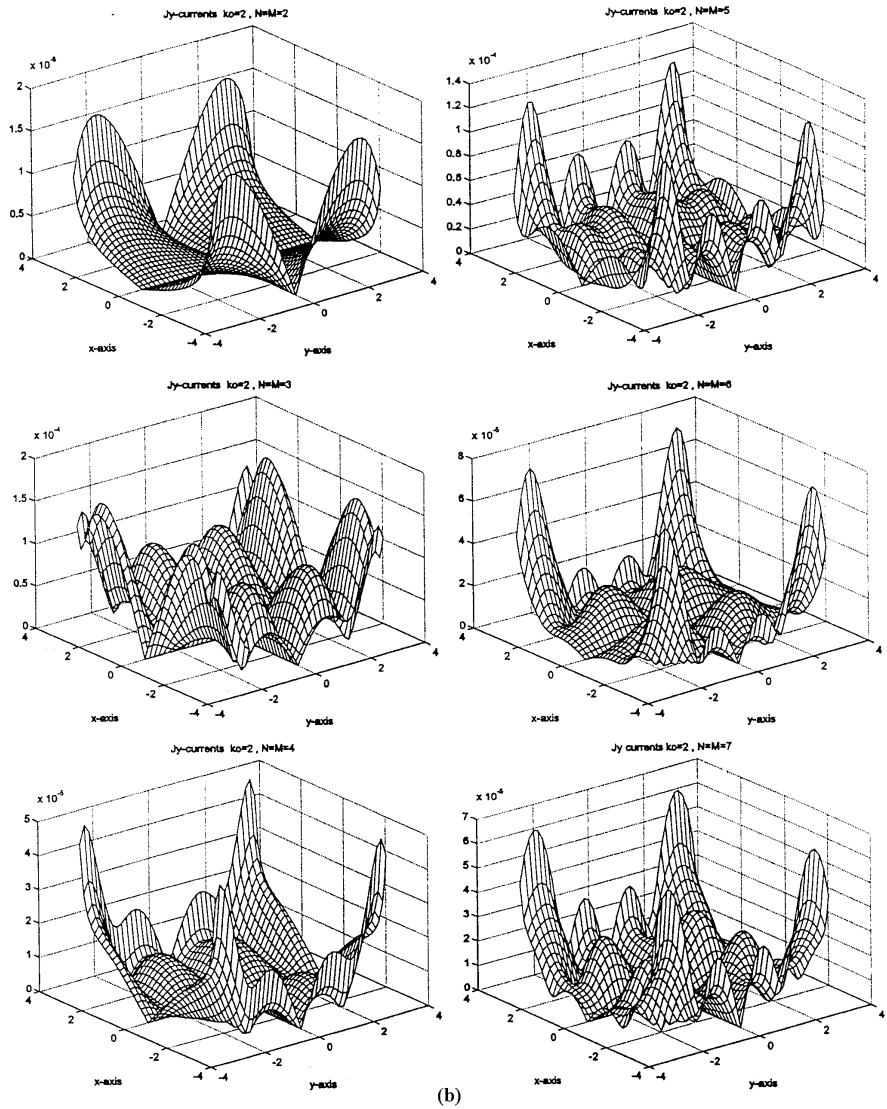

Figure 4. Convergence of the conductivity currents induced on each plate of the open resonator shown in Figure 1(a), for $k_0 = 2$: (b) cross-polarised $|J_y|$ currents.

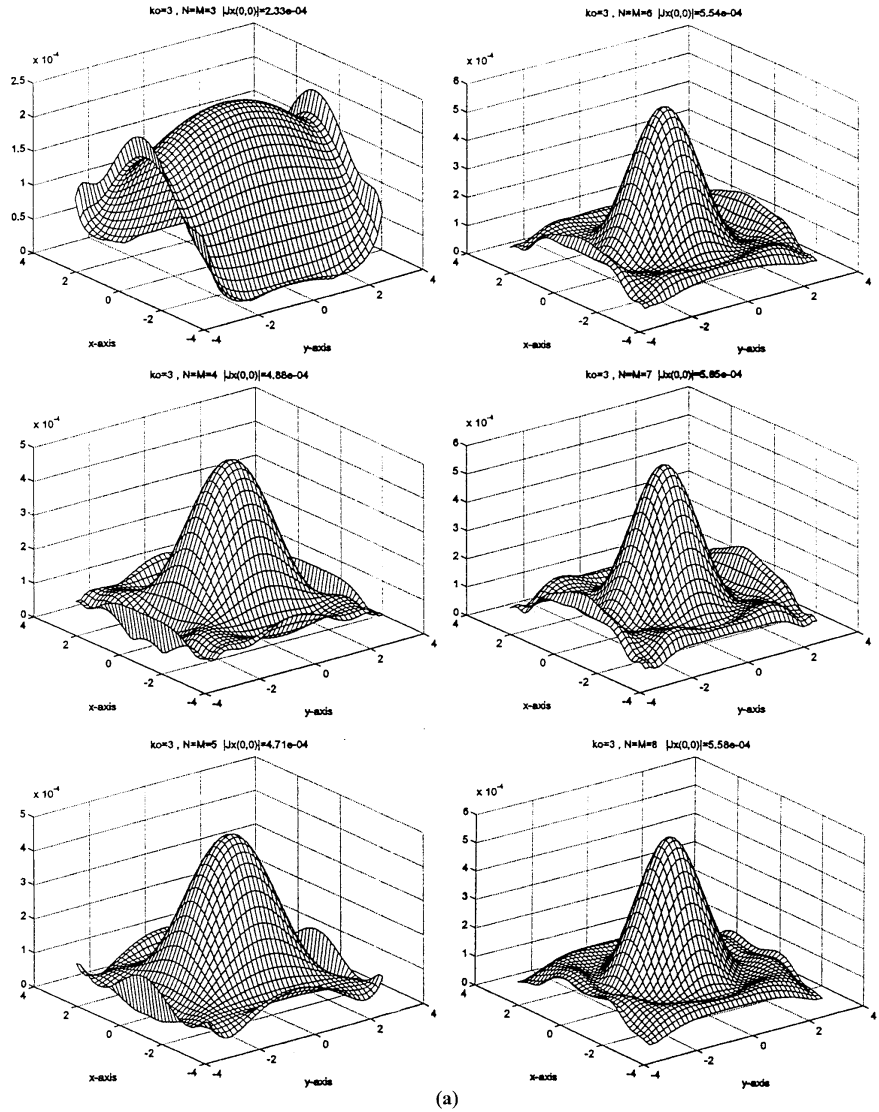

Figure 5. Convergence of the conductivity currents induced on each plate of the open resonator shown in Figure 1(a), for $k_0 = 3$: (a) co-polarised $|J_x|$ currents.

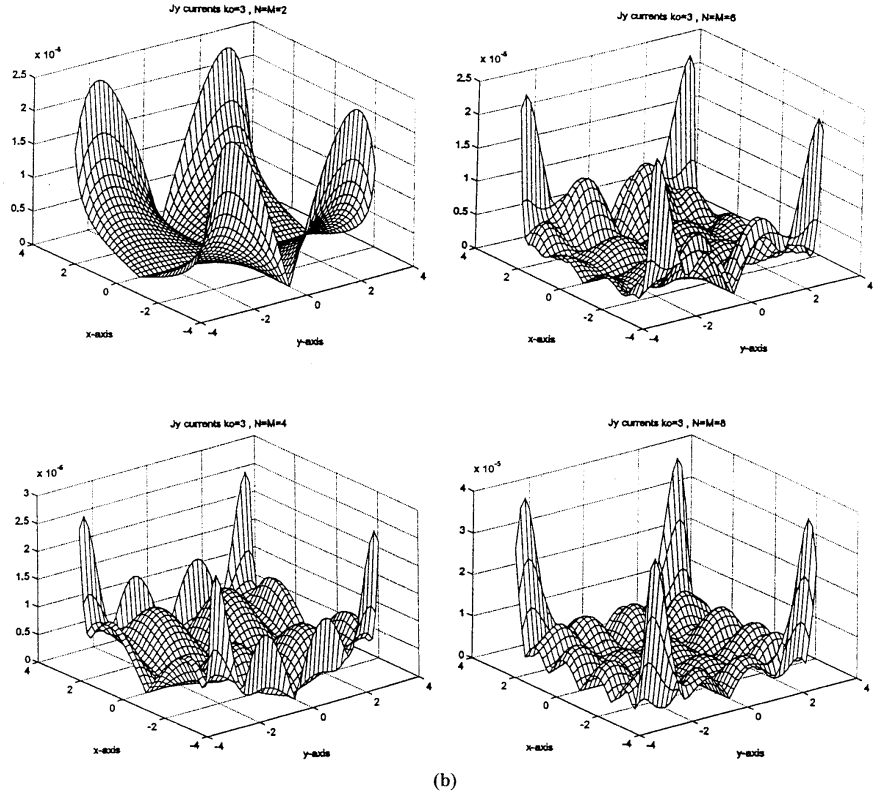

(b)

Figure 5. Convergence of the conductivity currents induced on each plate of the open resonator shown in Figure 1(a), for $k_0 = 3$: (b) cross-polarised $|J_y|$ currents.

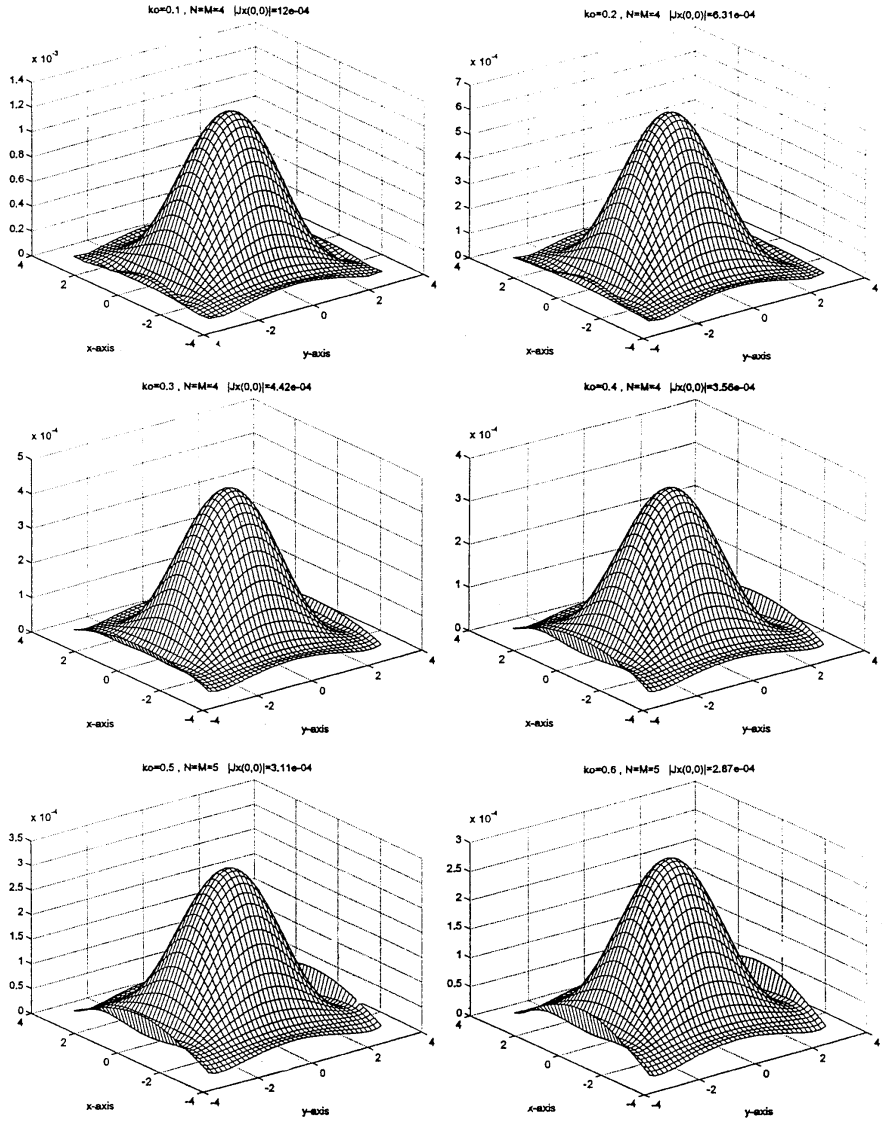

Figure 6. Co-polarised conductivity currents distribution induced on each plate of the open resonatoor shown in Figure 1(a), for the frequency region $k_0 = 0.1$ to 2.0 ($|J_x(0,0)| = \max|J_x|$).

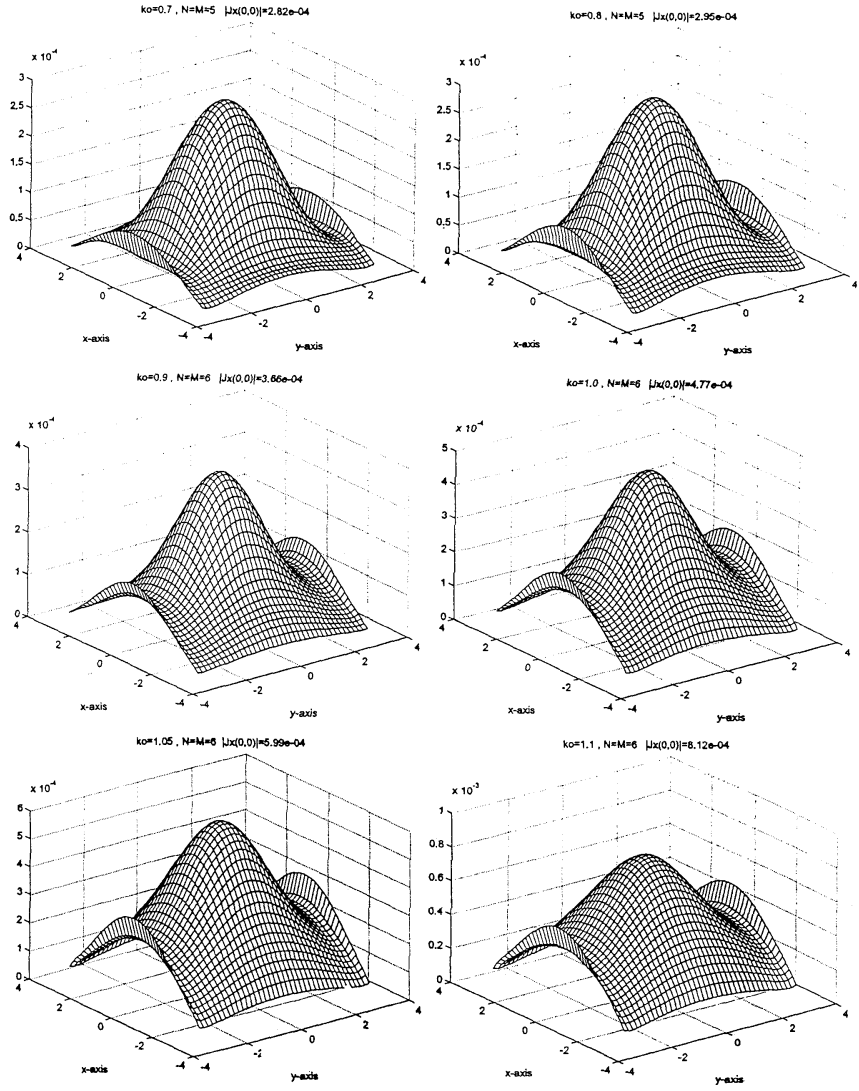

Figure 6. Co-polarised conductivity currents distribution induced on each plate of the open resonatoor shown in Figure 1(a), for the frequency region $k_0 = 0.1$ to 2.0 ($|J_x(0,0)| = \max|J_x|$).

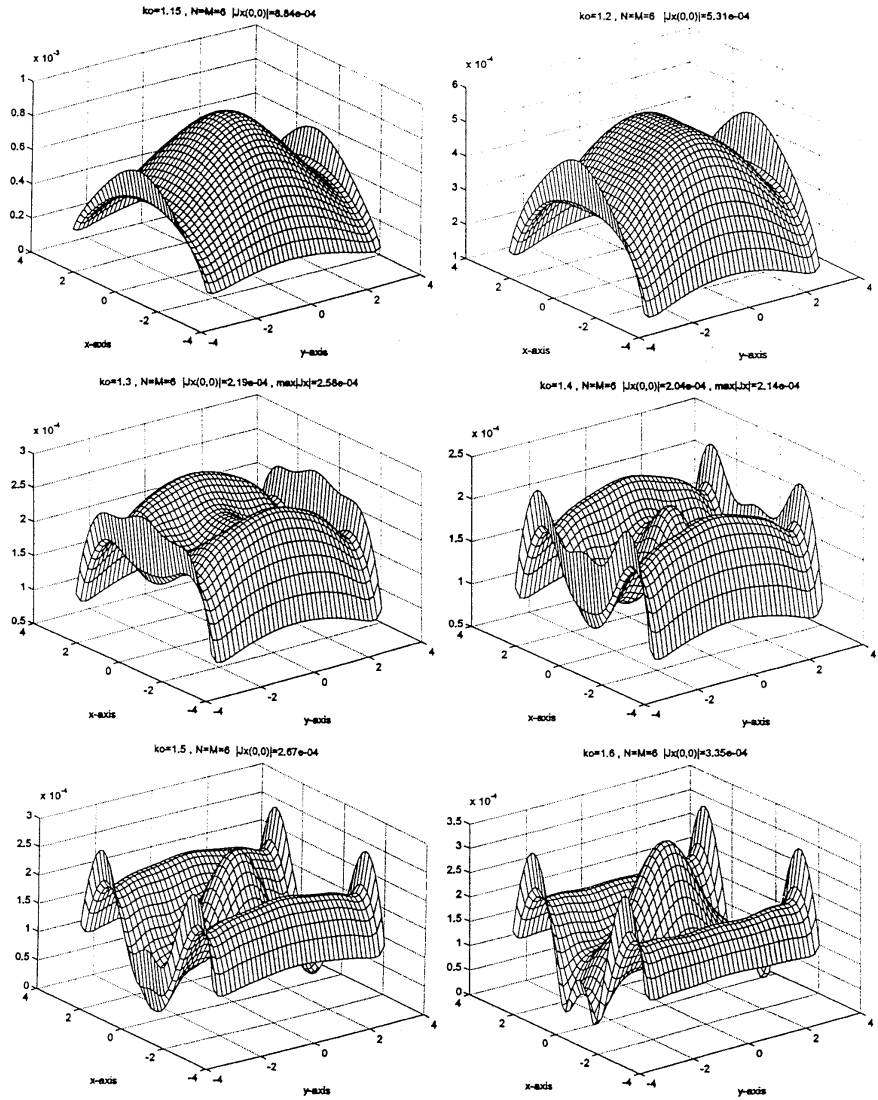

Figure 6. Co-polarised conductivity currents distribution induced on each plate of the open resonatoor shown in Figure 1(a), for the frequency region $k_0 = 0.1$ to 2.0 ($|J_x(0,0)| = \max|J_x|$).

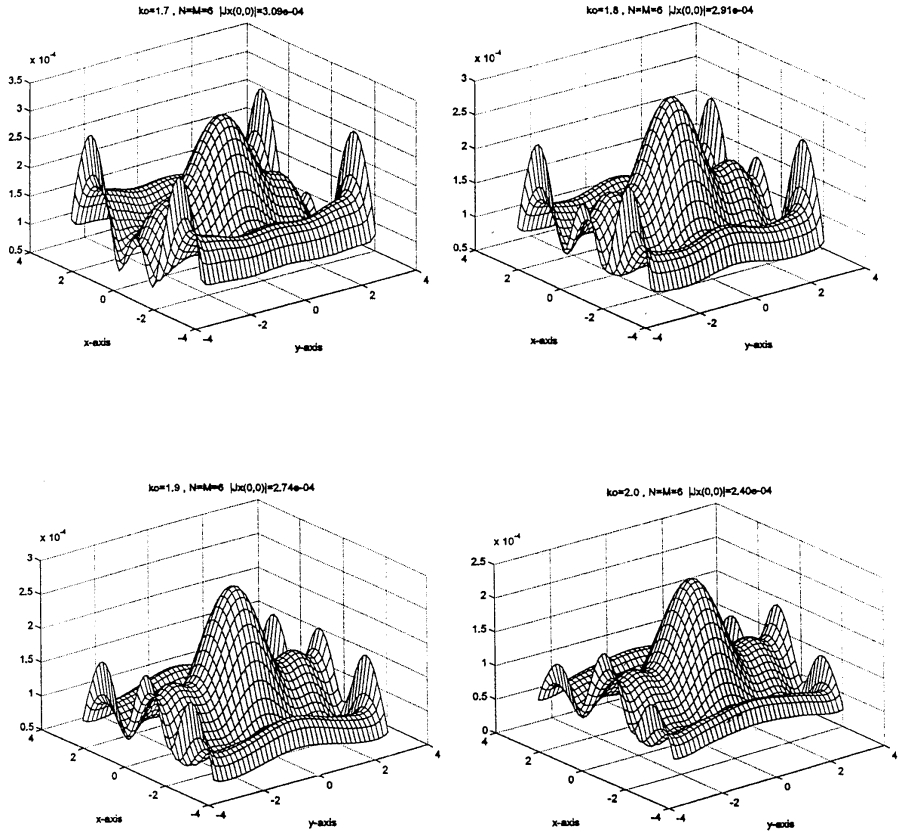

Figure 6. Co-polarised conductivity currents distribution induced on each plate of the open resonatoor shown in Figure 1(a), for the frequency region $k_0 = 0.1$ to 2.0 ($|J_x(0,0)| = \max|J_x|$).

Finally, in order to prove the applicability of the developed code to diverse structures of the type shown in Figure 1(b), indicative convergence results are presented in Figure 8 concerning a plane wave incidence $\underline{E}_0(\underline{r}) = \hat{x}\exp(-jk_0\hat{z}\cdot\underline{r})$ on two plates lying on the same xy-plane $(z_2^0 = z_1^0 = 0)$. Additionally, the 2nd plate is tilled with respect to the 1st one, as shown in Figure 8(a) and, therefore the angle φ has to be taken into account in all the involved calculations. As far as that 1st plate $2\lambda \times 2\lambda$ is concerned, only the dominant co-polarised x-currents are plotted in Figure 8(b), which serve also as an independent check of the proposed method by comparing with previously published

data [23, 35], while as far as the 2nd plate $\lambda \times \lambda$ is concerned, both x- and y- currents are significant due to the φ angle and their convergence is exhibited in Figures 8(c) and (d) respectively. Note that, the latter current distributions on the 2nd plate are plotted with respect to the local cartesian coordinates system (x_2, y_2), attached to the 2nd plate centre of gravity.

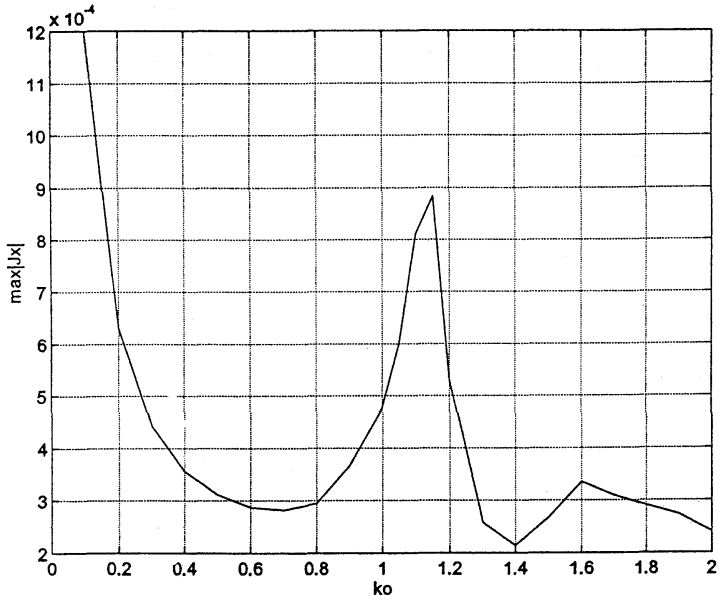

Figure 7. Max $|J_x|$ distribution in the frequency region $k_0 = 0.1$ to 2.0 for the open resonator shown in Figure 1(a).

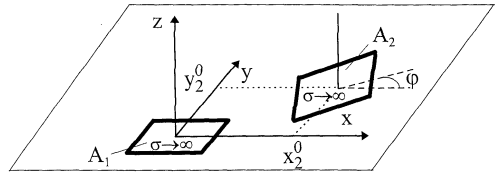

(a)

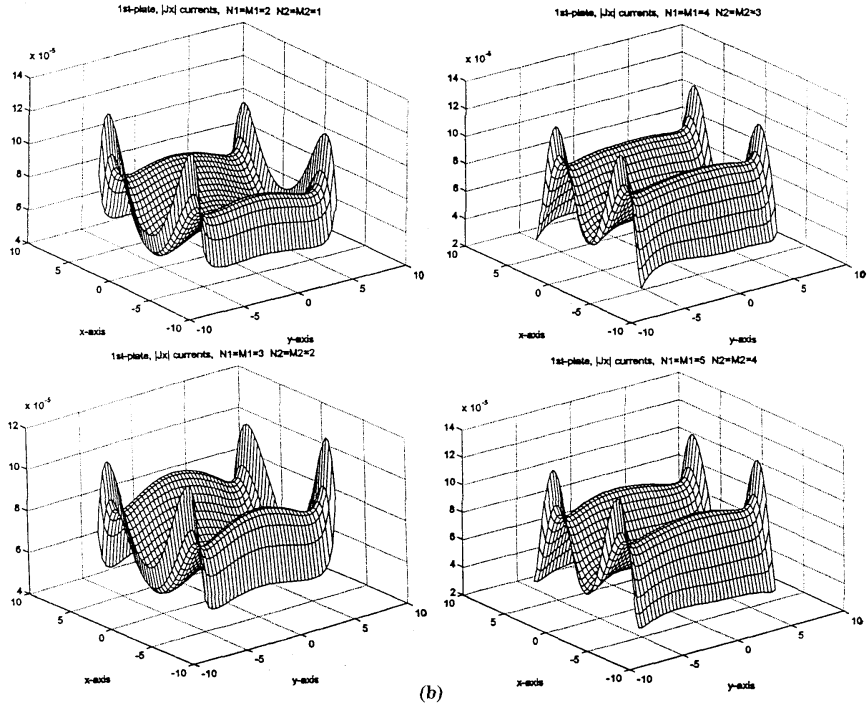

(b)

Figure 8. Plane wave incidence $\underline{E}_0(\underline{r}) = \hat{x}\exp(-jk_0\hat{z}\cdot\underline{r})$ on two plates lying on the same xy-plane, the 2nd one being tilled with respect to the 1st one: (a) geometry: $z_2^0 = z_1^0 = 0$, $x_2^0 = y_2^0 = 2\lambda$, $a_1 = b_1 = 2\lambda$, $a_2 = b_2 = \lambda$, $\varphi = 45^o$ (b) convergence of the $|J_x|$ currents induced on the 1st plate.

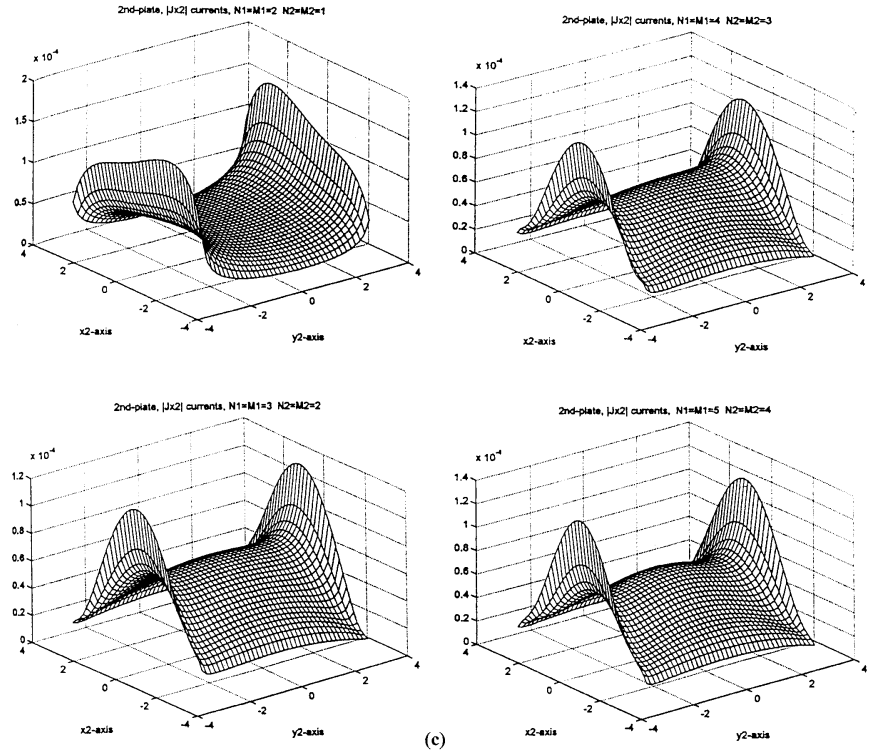

Figure 8. Plane wave incidence $\underline{E}_0(\underline{r}) = \hat{x}\exp(-jk_0\hat{z}\cdot\underline{r})$ on two plates lying on the same xy-plane, the 2nd one being tilled with respect to the 1st one: (c) convergence of the $|J_x|$ currents induced on the 2nd plate,

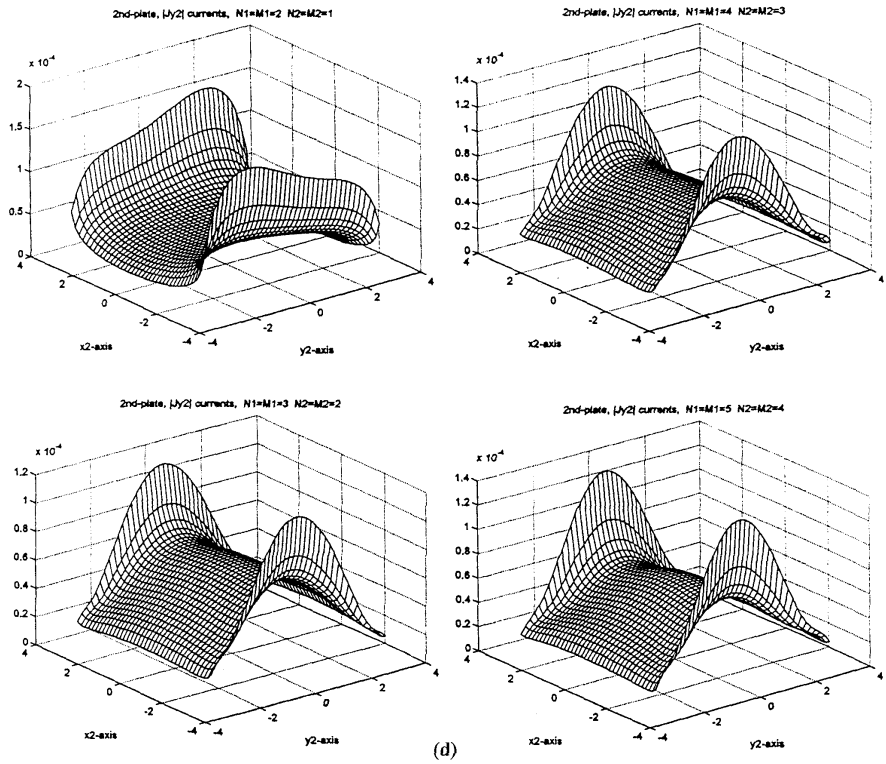

Figure 8. Plane wave incidence $\underline{E}_0(\underline{r}) = \hat{x}\exp(-jk_0\hat{z}\cdot\underline{r})$ on two plates lying on the same xy-plane, the 2nd one being tilled with respect to the 1st one: (d) convergence of the $|J_y|$ currents induced on the 2nd plate.

5. CONCLUSIONS–FUTURE WORK

The resonance properties of a parallel-plates open resonator have been examined, using an integral equation formulation in conjunction with a moment method with entire domain Chebychev type Galerkin expansions. Several different geometries concerning the plates dimensions and relative position and/or the dipole-plates relative positions have been investigated.

Knowledge of the Hertzian dipole effect (Green's function) is a fundamental stage in analysing other not-elementary source types, while the pursued analysis can be easily extended to the case of multi Fabry-Perot resonators, taking into account coupling phenomena between

closely spaced resonators. Furthermore, once the multi-plate problem shown in Figure 1(b) is solved, more complex conducting structures could be constructed. To this end, other shapes such as rhombs, trapezoids or polygonals will be additionally examined in the future, together with the "corner" problem, in order to construct more complicated —in terms of geometry— configurations.

MATHEMATICAL APPENDIX

The analytical expressions of the system (17) kernel elements are defined as

$$\overline{\underline{X\Psi}}_{pq}(n,m,n',m') = \frac{\omega\mu_0}{8\pi^2 k_0^2}\iint\limits_{\Omega_k} d\underline{\tilde{k}}\,\frac{e^{-j[q_0\mathrm{sgn}(z_p^0-z_q^0)(z_p^0-z_q^0+\delta_p)+k_x(x_q^0-x_p^0)+k_y(y_q^0-y_p^0)]}}{q_0} \overline{\underline{U}}_{p_{n'm'}}(-\underline{\tilde{k}})\cdot\overline{\underline{A}}(\underline{\tilde{k}})\cdot\overline{\underline{U}}_{q_{nm}}(\underline{\tilde{k}}) \tag{A.1}$$

where ($q = 1,2,\ldots,Q$; $p = 1,2,\ldots,Q$), $\underline{r}_q^0 = x_q^0\hat{x}+y_q^0\hat{y}+z_q^0\hat{z}$ denotes the position vector of the q-th plate centre of gravity with respect to a global system of coordinates (x,y,z), $\delta_p \to 0^+$, $\underline{\tilde{k}}$ and $q_0 = q_0(\underline{\tilde{k}})$ are defined by eqs (15) and (16) respectively,

$$\overline{\underline{U}}_{q_{nm}}(\underline{\tilde{k}}) = \frac{(n+1)J_{n+1}(-\frac{k_x a_q}{2})J_m(-\frac{k_y b_q}{2})}{2j^{(n+m)}k_x/(b_q\pi^2)}\hat{x}\hat{x}+ \frac{(m+1)J_{m+1}(-\frac{k_y b_q}{2})J_m(-\frac{k_x a_q}{2})}{2j^{(n+m)}k_y/(a_q\pi^2)}\hat{y}\hat{y} \tag{A.2}$$

and

$$\overline{\underline{A}}(\underline{\tilde{k}}) = \overline{\underline{A}}(\rho_k,\phi_k) = (k_0^2-k_x^2)\hat{x}\hat{x} - k_x k_y(\hat{x}\hat{y}+\hat{y}\hat{x}) + (k_0^2-k_y^2)\hat{y}\hat{y} \tag{A.3}$$

As far as the right hand side of eq. (17) is concerned, if the excitation consists of an elementary horizontal Hertzian dipole defined by eqs (1)–(3), it is valid that

$$\underline{X\Psi}_p^0(n'm') = -\frac{j}{8\pi^2 k_0^2}\iint\limits_{\Omega_k} d\underline{\tilde{k}}\,\frac{e^{-j[q_0\mathrm{sgn}(\delta-z_p^0)(\delta-z_p^0-\delta_p)+\rho_k(\underline{r}_0\cdot\hat{\delta})]}}{q_0} \underline{R}(\underline{\tilde{k}})\cdot\overline{\underline{U}}_{p_{n'm'}}(-\underline{\tilde{k}}) \tag{A.4}$$

where $\underline{R}(\tilde{\underline{k}}) = k_0^2\hat{\delta} - (\tilde{\underline{k}} \cdot \hat{\delta})\tilde{\underline{k}}$, while, if a plane wave defined by eq. (4) illuminates the multi-plate conducting structure, it is valid that

$$\underline{\underline{X}}\Psi_p^0(n'm') = \hat{e}\exp\Big[-jk_0\hat{k}_i \cdot (\underline{r}_p^0 + \delta_p\hat{z})\Big] \cdot \overline{\underline{U}}_{p_{n'm'}}(k_0\hat{k}_i) \qquad \text{(A.5)}$$

ACKNOWLEDGMENT

The author would like to thank Mr. Konstantinos Adam for his assistance in obtaining the numerical results presented in Figures 2–8.

REFERENCES

1. Fox, A. G., and T. Li, "Resonant modes in a maser interferometer," *Bell Syst. Tech. Jour.,* Vol. 40, 453–458, March 1961.
2. Schawlow, A. L., and C. H. Townes, "Infrared and optical masers," *Phys. Rev.,* Vol. 112, 1940–1949, Dec. 1958.
3. Jenkins, F. A., and H. E. White, *Fundamentals of Optics*, 3rd ed., McGraw-Hill, New York, 1957.
4. Wait, J. R., *Electromagnetic Waves in Stratified Media*, Pergamon Press, New York, 1962.
5. Born, M., and E. Wolf, *Principles of Optics*, 6th ed., Pergamon Press, Oxford, 1980.
6. Haus, H. A., *Waves and Fields in Optoelectronics*, Prentice-Hall, Inc., Englewood Cliffs, New Jersey, 1984.
7. McCleary, J., M. -Y. Li, and K. Chang, "Ka-band slot-fed higher order mode low-loss Fabry-Perot filters," *IEEE Trans. Microwave Theory Tech.,* Vol. MTT-42, 1423–1426, July 1994.
8. Sanagi, M., E. Yamamoto, S. Nogi, and R. G. Ranson, "Axially symmetric Fabry-Perot power combiner with active devices mounted on both the mirrors," *IEEE MTT–S Digest,* 1259–1262, 17–21 June 1996.
9. Dryagin, Y. A., V. V. Parshin, A. F. Krupnov, N. Gopalsami, and A. C. Raptis, "Precision broadband wavemeter for millimeter and submillimeter range," *IEEE Trans. Microwave Theory Tech.,* Vol. MTT-44, 1610–1613, Sept. 1996.
10. Fujii, T., H. Mazaki, F. Takei, J. Bae, M. Narihiro, T. Noda, H. Sakaki, K. Mizuno, and R. G. Ranson, "Coherent power combining of millimeter wave resonant tunneling diodes in a quasi-optical resonator," *IEEE MTT-S Digest,* 919–922, 17–21 June 1996.
11. De Melo, M. T., M. J. Lancaster, H. Yokota, and C. E. Gough, "High temperature superconducting microstrip resonators for the

measurement of films made by pyrolysis," *Proc. 1995 SBMO/IEEE MTT-S,* 868–872, 24–27 July 1995.
12. Mourachkine, A. P., and A. R. F. Barel, "Microwave measurement of surface resistance by the parallel-plate dielectric resonator method," *IEEE Trans. Microwave Theory Tech.,* Vol. MTT-43, 544–551, March 1995.
13. Gevorgian, S., E. Carlsson, P. Linner, E. Kollberg, O. Vendik, and E. Wikborg, "Lower order modes of YBCO/STO/YBCO circular disk resonators," *IEEE Trans. Microwave Theory Tech.,* Vol. MTT-44, 1738–1741, Oct. 1996.
14. Feng, G., M. V. Klein, J. Kruse, and M. Feng, "Mode coupling in superconducting parallel plate resonator in a cavity with outer conductive enclosure," *IEEE Trans. Microwave Theory Tech.,* Vol. MTT-44, 944–952, June 1996.
15. Farber, E., G. Deutscher, G. Koren, and E. Jerby, "Microwave measurements of high Tc superconductors," *1996 9th Conv. Electrical and Electronics Eng. in Israel,* 444–447, 5–6 Nov. 1996.
16. Roan, G. T., and K. A. Zaki, "Calculation of losses in a superconductive resonator using FDTD," *IEEE AP-S Digest,* 384–387, 13–18 July 1997.
17. Casimir, H. B. G., and D. Polder, "The influence of retardation on the London — van den Waals Forces," *Physical Review,* Vol. 73, 360–372, 1948.
18. Casimir, H. B. G., "On the attraction between two perfectly conducting plates," *Proc. Kon. Ned. Akad. Wetensch B51,* Vol. 60, 793, 1948.
19. Lamoreaux, S. K., "Demonstration of the Casimir Force in the 0.6 to 6 μm range," *Physical Review Letters,* Vol. 78, No. 1, 5–8, 1997, and "Erratum: Demonstration of the Casimir Force in the 0.6 to 6 μm range," *Physical Review Letters,* Vol. 81, No. 24, 5475–5476, 1998.
20. Kaklamani, D. I., and A. Marsh, "Benchmarking high performance computing platforms in analyzing electrically large planar conducting structures via a parallel computed Method of Moments technique," *Radio Sci.,* Vol. 31, 1281–1290, Sept. – Oct. 1996.
21. Kaklamani, D. I., K. S. Nikita, and A. Marsh, "Extension of method of moments for electrical large structures based on parallel computations," *IEEE Trans. Antennas Propagat.,* Vol. AP-45, 566–568, March 1997.
22. Marsh, A., D. I. Kaklamani, and K. Adam, "Using parallel processing as a computational tool to solve multi-plate electromagnetic scattering problems," accepted for publication in *Parallel*

Processing Letters.
23. Kaklamani, D. I., and A. Marsh, "Solution of electrically large planar scattering problems using parallel computed method of moments technique," *J. Electro. Waves Applic.,* Vol. 9, 1313–1337, 1995.
24. Meixner, J., "The behavior of electromagnetic fields at edges," *IEEE Trans. Antennas Propagat.,* Vol. AP-20, 442–446, 1972.
25. Kaklamani, D. I., and N. K. Uzunoglu, "Scattering from a conductive rectangular plate covered by a thick dielectric layer and excited from a dipole or a plane wave," *IEEE Trans. Antennas Propagat.,* Vol. AP-42, 1065–1076, 1994.
26. Harrington, R. F., *Field Computation by Moment Methods,* New York: Macmillan, Florida: Krieger Publishing, 1983.
27. Sarkar, T. K., A. R. Djordjevic, and E. Arvas, "On the choice of expansion and weighting functions in the numerical solution of operator equations," *IEEE Trans. Antennas Propagat.,* Vol. AP-33, 988–996,1985.
28. Aksun, M. I., and R. Mittra, "Choices of expansion and testing functions for the Method of Moments applied to a class of electromagnetic problems," *IEEE Trans. Microwave Theory Tech.,* Vol. MTT-41, 503–509, 1993.
29. Coen, G., N. Fache, and D. De Zutter, "Comparison between two sets of basis functions for the current modelling in the galerkin spectral domain solution for microstrips," *IEEE Trans. Microwave Theory Tech.,* Vol. MTT-42, 505–513, 1994.
30. Alanen, E., "Pyramidal and entire domain basis functions in the method of moments," *J. Electro. Waves Applic.,* Vol. 5, 315–329, 1991.
31. Pozar, D. M., "A reciprocity method of analysis for printed slot and slot-coupled microstrip antennas," *IEEE Trans. Antennas Propagat.,* Vol. AP-34, 1439–1446, 1989.
32. Sarkar, T. K., S. M. Rao, and A. R. Djordjevic, "Electromagnetic scattering and radiation from finite microstrip structures," *IEEE Trans. Antennas Propagat.,* Vol. AP-38, 568–1575, 1990.
33. Abramowitz, M., and I. A. Stegun, *Handbook of Mathematical Functions,* Dover Publications, Inc., New York, 1970.
34. Kaklamani, D. I., "Analysis of dielectric-loaded radiation structures," Ph.D. Dissertation, National Technical University of Athens, Athens, 1992 (in Greek).
35. Volakis, J. L., and K. Barkeshli, "Applications of the conjugate gradient method to radiation and scattering," *Application of Iterative Methods to Electromagnetics and Signal Processing,* Ch. 4, ed. K. Sarkar, Elsevier Science Publishing Co., 1991.